Tropospheric mixing and parametrization of unresolved convection as implemented into the Chemical Lagrangian Model of the Stratosphere (CLaMS)

Paul Konopka, Mengchu Tao, Felix Ploeger, Mohamadou Diallo, and Martin Riese

Forschungszentrum Jülich, (IEK-7), Germany

Correspondence to: Paul Konopka (p.konopka@fz-juelich.de)

Abstract. Inaccurate representation of mixing in chemistry transport model, mainly suffering from an excessive numerical diffusion, strongly influences the quantitative estimates of the stratosphere-troposphere exchange (STE). The Lagrangian view of transport offers an alternative to exploit the numerical diffusion for parametrization of the physical mixing. Here, we follow this concept and discuss how to extend the representation of tropospheric transport in the Chemical Lagrangian Model of the

5   Stratosphere (CLaMS).

Although the current transport scheme in CLaMS shows good ability of representing transport of tracers in the stably strat-ified stratosphere (Pommrich et al. (2014) and the references therein), there are deficiencies in representation of the effects of convective uplift and mixing due to weak vertical stability in the troposphere. We show how the CLaMS transport scheme was modified by including additional tropospheric mixing and vertical transport due to unresolved convection by parametrizing

10   these processes in terms of the dry and moist Brunt-Väisälä frequency, respectively. The regions with enhanced vertical trans-port in the novel CLaMS simulation covering the 2005-08 period coincide with regions of enhanced convection as diagnosed from the satellite observations of the Outgoing Longwave Radiation (OLR) .

We analyze how well this approach improves the CLaMS representation of CO_2 in the upper troposphere and lower strato-sphere, in particular the propagation of the CO_2 seasonal cycle from the Planetary Boundary Layer (PBL) into the lower

15   stratosphere. The CO_2 values in the PBL are specified by the CarbonTracker data set (version CT2013B) and the Compre-hensive Observation Network for TRace gases by AIrLiner (CONTRAIL) observations are used to validate the model. The proposed extension of tropospheric transport increases the tropospheric influence in the middle and upper troposphere and at the same time influences the STE. The effect on mean age away from the troposphere in the deep stratosphere is weak.

1   Introduction

20   Modeling of transport from a Lagrangian perspective has gained increasing popularity in the last few decades not only within the atmospheric community. The chance to avoid, or at least to minimize, the numerical diffusion ever present in Eulerian numerical schemes is the strongest motivation for the Lagrangian formulation of transport. Despite the obvious advantage of the Lagrangian view separating mixing from the advective part of transport, only very few Lagrangian chemical transport

models (CTMs) with explicit mixing exist so far (e.g. Collins et al., 1997; Fairlie et al., 1999; Reithmeier and Sausen, 2002; McKenna et al., 2002b; Konopka et al., 2007; Wohltmann and Rex, 2009; Pugh et al., 2012).

In this paper, the 3D version of the Chemical Lagrangian Model of the Stratosphere (CLaMS) will be used (McKenna et al., 2002b, a; Konopka et al., 2004). The novel approach of CLaMS is its parametrization of atmospheric mixing, especially in the stratosphere where vertical mixing is extremely weak due to a strong vertical stability. Whereas the common approach is to

5 minimize the numerical diffusion ever present in the modeling of transport, CLaMS is a first attempt to apply this "undesirable disturbing effect" to parametrize the "true" physical mixing. This idea is realized by using some scaling properties of numerical diffusion, which are the same as of the atmospheric diffusivity (Konopka et al., 2007, 2012; Pommrich et al., 2014) and by applying numerical regridding only to the strongly deformed parts of the Lagrangian grid where physical mixing is expected anyway (McKenna et al., 2002b; Konopka et al., 2004). This novel parametrization of mixing was included into the well-known

10 pure Lagrangian, i.e., trajectory-based representation of transport (e.g. Stohl et al., 2005; Legras et al., 2005; Bowman et al., 2007; Wernli and Davies, 1997).

However, in the current version of CLaMS (Pommrich et al., 2014) only deformations within quasi-isentropic layers driven by horizontal strain and vertical shear rates are taken into account. This is certainly a good approximation in a stably stratified stratosphere suppressing vertical mixing but not in the troposphere where vertical mixing is expected. To extend the CLaMS

15 idea of "sufficiently strong", almost isentropic deformations triggering mixing to the troposphere we use the concept of atmospheric stability. The flow is called unstable if a small perturbation at initial time will exponentially grow during the course of the evolution of the flow.

One of the widely used parameters quantifying instabilities is the gradient Richardson number, Ri_c describing the onset of instabilities driven by wind shear and/or buoyancy (e.g. Turner, 1973; Stull, 1988). Ri is defined as $Ri = N^2/[(du/dz)^2 +$

20 $(dv/dz)^2]$ with du/dz, dv/dz denoting the vertical shear of the horizontal wind components. N is the (dry) Brunt Vaisala frequency quantifying buoyancy-driven turbulence in terms of the potential temperature lapse rate, i.e. $N^2 = (g/\theta)d\theta/dz$ (θ - potential temperature, g - gravity of Earth and z geometric altitude). The scale-dependent value of Ri_c, is about 0.25 although reported values have ranged from roughly 0.2 to 1.0 (Balsley et al., 2008). The flow becomes dynamically unstable or even turbulent when $Ri < Ri_c$. This occurs either when the wind shear is great enough to outweigh any stabilizing buoyant forces

25 (denominator in the definition of Ri is large), or when the dry or, more general, moist environment is statically unstable (numerator in the definition of Ri is small or even negative because the lapse rate $d\theta/dz$ is small or even negative).

In the stratosphere, where the flow is characterized by high static stability, only almost isentropic deformations driven by the horizontal strain and vertical shear are detected in the current version of CLaMS (Pommrich et al. (2014) and the references therein). These deformations measured in terms of the Lyapunov exponent λ are used in CLaMS to parametrize mixing within

30 layers, which are parallel to the isentropes roughly about 300 hPa. However, the effect of vertical instabilities being a dominant feature of tropospheric transport is not taken into account. To parametrize such (potentially) vertically unstable regions by using "sufficiently small" values of the dry or moist Brunt Vaisala frequency N or N_m is our main heurestic idea, how to generalize the CLaMS mixing scheme in the troposphere.
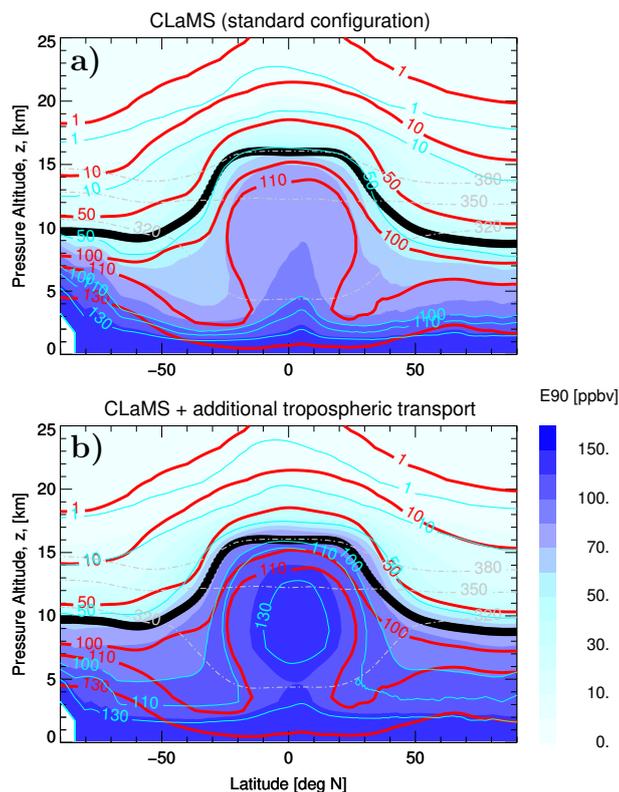
Figure 1. The different shades of blue quantify the annual mean of the e90 tracer mixing ratios (calculated for 2007) as a function of latitude and log-pressure altitude and are derived from the current version of CLaMS described in Pommrich et al. (2014) (a) and from the here discussed version with extended tropospheric transport (b). For comparison, the WACCM 1955-2099 climatology of e90 is also shown (red isolines) as described in Abalos et al. (2017). The mean tropopause and few selected isentropes are depicted by black and dashed gray lines, respectively .

Generally, CLaMS tropospheric tracers like CO or CH_4 show reasonably mixing ratios in the Upper Troposphere and Lower
35 Stratosphere (UTLS) only if their values in the lowest model boundary are artificially enhanced by a factor 1.5-2 (Pommrich et al., 2014). The consequence of this enhancement are too strong vertical gradients of these tracers, especially in the lower and middle troposphere if compared with observations (not shown). A possible reason might be that a significant part of the upwards vertical transport within the troposphere is underestimated.

Figure 1 shows a comparison in terms of the e90 tracer between the current CLaMS version (top), the here discussed
5   extension of tropospheric transport (bottom) with the Whole Atmospheric Community Climate Model (WACCM, red isolines) which is known for a good representation of tropospheric transport and chemistry (see e.g. Park et al. (2013) and the references therein). Here, the CLaMS annual means (calculated for 2007) are compared with the WACCM 1955-2099 climatology.

Similar like in WACCM, the artificial tracer e90, with a constant e-folding lifetime of 90 days, is set to 150 ppb everywhere in the lowest layer of CLaMS. The e90 tracer is suitable to diagnose typical timescale of transport from the Planetary Boundary Layer (PBL) into the lower stratosphere (Prather et al., 2011; Abalos et al., 2017). Figure 1 shows that CLaMS in the current version significantly underestimates the upward transport if compared with the WACCM model and that this comparison improves if the new version of transport is included.

In this paper, we aim to parametrize the unresolved subgrid processes like convection and tropospheric mixing whose representation in global reanalysis data is uncertain (Russo et al., 2011). Although we are aware of numerous convective schemes (e.g. Tiedtke (1989); Emanuel (1991)), our approach mainly intends to cover the range of possible variability due to unresolved tropospheric transport. In particular, we aim here to create a technical framework which allows us in the future to estimate the impact of such uncertainties on the composition of the UTLS as well as on the Stratosphere-Troposphere-Exchange (STE). Even small changes in the concentration and distribution of radiatively active gases in the UTLS such as water vapor or ozone significantly impact radiative forcing on surface temperature (Riese et al. (2012), IPCC2014).

In the next section, we describe, the properties and mean distributions of the dry or moist Brunt Vaisala frequency N or N_m as derived from the meteorological data. N and N_m are used in this paper to parametrize the additional tropospheric transport. Section 3 explains technical details of this parametrization. Section 4 describes the CLaMS setup, details of the performed model runs as well as some results diagnosing which regions of the atmosphere are mainly affected by our extension of transport. To validate these new properties we discuss the transport of CO_2 from the PBL into the lower stratosphere and compare the respective distributions with the airborne observations and the CarbonTracker model simulations. Finally, we discuss our results in section 5.

2 Vertically unstable troposphere versus stably stratified stratosphere

Static stability can be quantified in terms of the (dry) Brunt-Vaisala frequency (BVF) via $N^2 = (g/\theta)(d\theta/dz)$. N describes the frequency at which an air parcel oscillates when displaced vertically in a statically stable environment, i.e. within a region with a positive lapse rate $d\theta/dz > 0$ (for some details see appendix A). Because the well-mixed troposphere is characterized by low values of N and the stably stratified stratosphere by high values of N, it is expected that this difference also manifests in the corresponding vertical diffusivities (large and small for the troposphere and the stratosphere, respectively).

To take into account the contribution of latent heat release to the vertical instabilities, N^2 can be modified by introducing the moist Brunt-Väisälä frequency N_m with $N_m^2 = (g/\theta_e)(d\theta_e/dz)$ where θ_e is equivalent potential temperature, i.e. the temperature an air parcel would reach if all the water vapor in the air parcel were to condense, releasing its latent heat and then were brought down adiabatically to 1000 hPa (for details see also appendix A). The zonal mean of the dry and moist BVF distribution during boreal winter and summer 2005 is exemplary shown in Fig. 2.

Thus, lowest values of the dry BVF are distinctive for the middle troposphere especially in the tropics. The minimum in lapse rate $d\theta/dz$ above the PBL represents the level of maximum convective impact (Gettelman and de Forster, 2002) which is also characterized by a vertically broad maximum of tropospheric signatures with enhanced CO and strongly reduced ozone
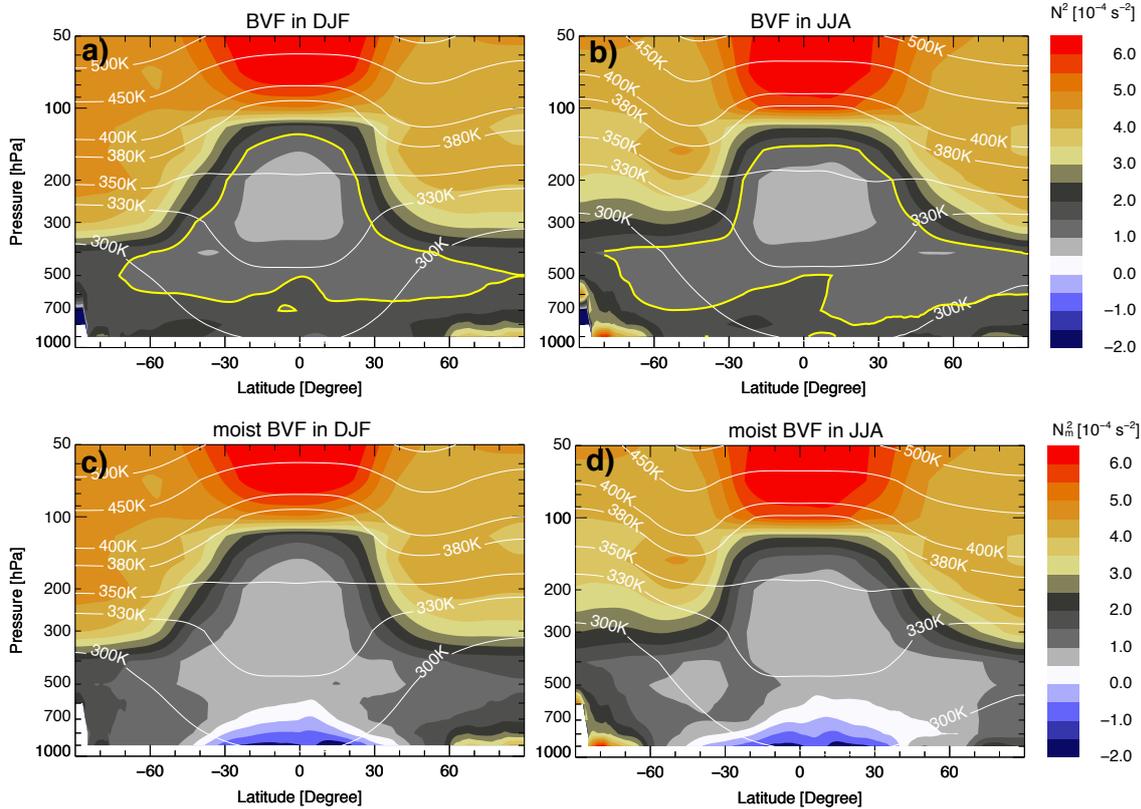
Figure 2. The zonal mean distribution of dry, N^2 (top) and moist, N_m^2 (bottom) Brunt-Väisälä frequency (BVF) in the troposphere and the lower stratosphere for DJF (a, c) and JJA (b, d) as calculated from 2005 ERA-Interim data. The thick yellow contours in the top row highlight those part of the atmosphere where the tropospheric mixing is included into CLaMS. The bluish colored regions in the bottom panels mark places from which additional parametrization of convection lifts the CLaMS air parcels from the PBL into the upper troposphere.

(Pan et al. (2017) and references therein). Obviously, the values of N^2 clearly increase by crossing the tropopause but they also increase in the region below 700 hPa and are the lowest in the tropical and sub-tropical middle troposphere (i.e. within the yellow contour in the top panel of Fig. 2) In the following section, we use this middle tropospheric minimum of N^2, although zonally-resolved, to parametrize tropospheric mixing in CLaMS and, in this way, to include unresolved mixing processes in the middle and upper troposphere into the CLaMS transport.

On the other hand, low values of the moist BVF (i.e. bluish regions with $N_m^2 < 0$ in the bottom panel of Fig. 2) can be found
5 at altitudes below 700 hPa between 30°S and 30°N, i.e. in the tropical and subtropical PBL. The air parcels with $N_m^2 < 0$ are conditionally unstable (see appendix A), i.e. they may undergo strong vertical uplift, if some other favorable conditions causing saturation may happen within such air masses (e.g. gravity wave-induced temperature fluctuations which is not resolved in the

meteorological data). In the following section, we show how conditional instability can be used to trigger additional (advective) upward transport due to unresolved convection.

3 Extension of transport scheme: tropospheric mixing and unresolved convection

5 To extend the CLaMS mixing scheme, we follow two heuristic ideas: First, due to a much lower vertical stability in the troposphere than in the stratosphere, we enhance tropospheric mixing in the model almost everywhere where (dry) vertical stability is sufficiently small. Second, we take into account additional transport driven by convection, especially by deep convection which is not sufficiently resolved in the reanalysis data.

Thus, whereas the first approach is related to changes in the mixing part of CLaMS and affects the next neighbors of each

10 Lagrangian air parcel, the second goal is related to changes in the advection part of CLaMS, i.e. to modification of the trajectory calculation. Both extensions should be driven by instabilities quantified in terms of the dry and moist BVF, respectively, which were introduced in the previous section. By including such a revised transport scheme, we seek for a better representation of transport in the free troposphere, which also likely improves the performance of the model within the UTLS region. Because all our changes are confined to the troposphere, we expect a weak influence on stratospheric transport in CLaMS which has been

15 successfully validated in many previous studies. Furthermore, the scheme should not give a heavy burden on the computation time compared to the current version of CLaMS. Before going into the details, we shortly describe the standard version of CLaMS (in the following denoted as the reference run).

3.1 Reference setup

As the reference, we use the 2005-2008 run of CLaMS (McKenna et al., 2002b; Konopka et al., 2004) driven by the horizontal

20 winds and diabatic heating rates (vertical velocities) derived from the ERA-Interim reanalysis (Dee et al., 2011; Ploeger et al., 2010). This configuration follows the model setup described in (Pommrich et al., 2014) (100 km horizontal/250 m vertical resolution around 380 K). Zonal mean distribution of the mean age of air (AoA), calculated relative to the Earth's surface is exemplarily shown for one day (19.08.2005) as the function of the latitude and the hybrid potential temperature ζ (top panel of Fig. 7) and will be used for comparison with CLaMS runs including the extended tropospheric transport (section 4).

25 The vertical coordinate ζ is the hybrid σ-θ which allows to resolve transport processes in the troposphere influenced by the orography and transport processes in the stratosphere where adiabatic horizontal transport dominates (Mahowald et al., 2002). More precisely, we replace η by σ in the hybrid η-θ coordinate as proposed by Mahowald et al. (2002), i.e.:

$$\zeta := f(\sigma)\theta(p,T), \tag{1}$$

with

$$f(\sigma) = \begin{cases} \sin\left(\frac{\pi}{2}\frac{1-\sigma}{1-\sigma_r}\right) & \sigma > \sigma_r \\ 1 & \sigma \le \sigma_r, \quad \sigma_r = \frac{p_r}{p_0} \end{cases} \tag{2}$$

Here, p_0 denotes the constant reference pressure level set to 1000 hPa. p_r defines the pressure level around which the potential temperature θ smoothly transforms into the terrain-following coordinate $\sigma = p/p_s$.

For p_r Mahowald et al. (2002) used the value 300 hPa, i.e. $\sigma_r = 0.3$. For situations with no orography (e.g. see surface with $p_s = 1000$ hPa) this means that the condition $\sigma = p/p_s < \sigma_r$ is valid everywhere above 300 hPa. Consequently, in this region the vertical coordinate ζ is given by the dry potential temperature θ. Conversely, below 300 hPa, θ smoothly transforms into σ.

5   For situations with orography (e.g. at the summit of Mount Everest with $p_s \approx 330$ hPa), the condition $\sigma = p/p_s < \sigma_r$ is first valid everywhere above ≈ 100 hPa. Note that all p_r values between 0 and 1000 hPa are possible with the consequence that higher p_r values extend the applicability of θ as a vertical coordinate down to the lower troposphere.

Thus, because ζ in the troposphere is a less intuitive coordinate (hybrid mixture between σ and θ), isolines of pressure and potential temperature as well as the zonal mean of the WMO tropopause are also shown in the top panel of Fig. 7. Furthermore,

10   vertical boundaries of the layers $\Delta\zeta_i$ within which CLaMS mixing is organized (for more details see Konopka et al. (2007)) are depicted at the left side. In the CLaMS reference run, the lowest layer $\Delta\zeta_0$ approximating the PBL extends between $\zeta = 0$ (Earth's surface) and 100 K, i.e. $\Delta\zeta_0 = \Delta\zeta_{pbl} = 100$K. After each trajectory step Δt, mixing ratios of all air parcels within this layer are replaced by their initial configuration and prescribed by a lower boundary condition.

In the default mixing scheme, CLaMS uses the integral deformations $\gamma = \lambda\Delta t$ derived from the relative motion of the next

15   neighbors within each layer $\Delta\zeta_i$ and λ being the Lyapunov exponent of such a deformation (adaptive grid procedure). In the stratosphere and in large parts of the UTLS, where the flow is characterized by a high static stability, only sufficiently strong deformations with $\gamma > \gamma_c$ (γ_c denoting an empirical critical deformation) are expected to trigger mixing with the best choice for γ_c between 0.8 and 1.5 (Konopka et al., 2004). This also means that there is some freedom in the choice of the parameters λ and Δt. Whereas for the stratosphere the values of $\Delta t = 24$ h and $\lambda = 1.5$ day^{-1} ($\gamma_c = 1.5$) were used in the past (Konopka

20   et al., 2004) (and are used here as the reference configuration), a larger mixing frequency with $\Delta t = 6$ h seems to give better results in the well-mixed troposphere and in the UTLS region (Vogel et al., 2011; Konopka and Pan, 2012).

3.2 Tropospheric mixing

In the following, we assume that the additional tropospheric mixing should be triggered whenever the corresponding value of N^2 interpolated at the CLaMS air parcel is less than a critical value denoted in the following as N_c^2. N_c^2 is a free parameter

25   which, basically, can be adjusted by comparison with the experimental data. We expect that N_c^2 should be around zero and should identify regions with (statistically) enhanced tropospheric mixing. If an air parcel fulfills the criterion $N^2 < N_c^2$, the air parcel will be mixed with all next neighbors diagnosed by Delaunay triangulation in the respective CLaMS layer under consideration (so we use the same next neighbors as in the standard CLaMS mixing scheme). In this way the composition of the considered air parcels are affected, but not their geometric positions.

30   Figure 3 is a schematic diagram illustrating how the tropospheric extension of mixing works. If this additional mixing is applied, we set the new mixing ratio of a considered air parcel and its next neighbors through averaging their composition, which is shown as a change of the parcel's color. This setting completes the mixing without changing any model parcel position
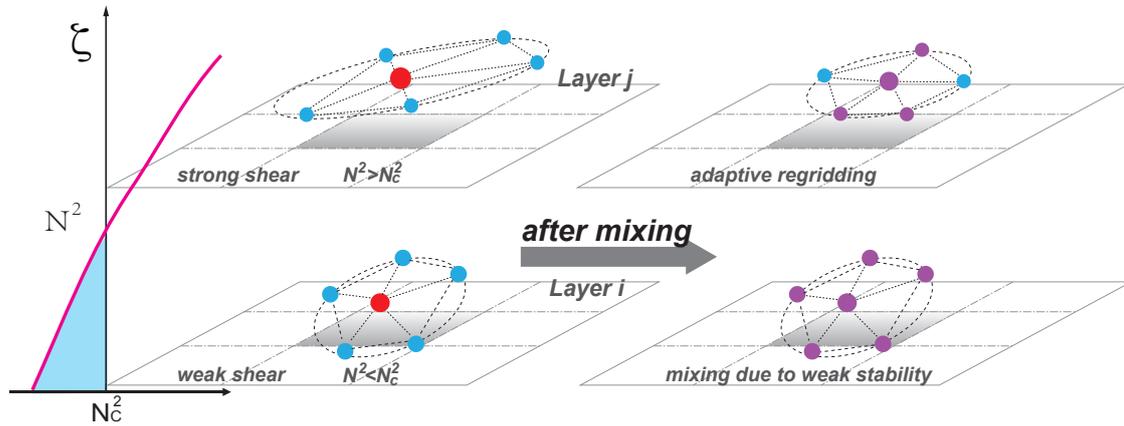
Figure 3. Mixing driven by vertical instability and strong wind shear. The profile on the left side is an idealized N^2 profile derived from the reanalysis and interpolated on the CLaMS air parcels (red). The lower part is representative for the troposphere with $N^2 < N_c^2$ and the upper part for the stratosphere with $N^2 > N_c^2$. Thus, in the lower layer static stability is weak with the opposite configuration in the upper layer where, in addition, the wind shear is strong. In the upper layer, adaptive regridding is used to include mixing between a subset of the next neighbors of the considered air parcel (default mixing in CLaMS). In addition, in the lower layer, all next neighbors will be mixed with the considered air parcel if criterion $N^2 < N_c^2$ is valid. The purple parcels are mixed parcels of red and blue parcels.

and the number of parcels because it can be executed directly in the current mixing module (more precisely, after deformation driven adaptive grid procedure of CLaMS).

3.3 Unresolved (deep) convection

5   It is generally believed that the exchange of mass driven by deep convection can efficiently inject the air masses from the PBL into the upper troposphere or even, although very rarely, into the lower stratosphere (Schiller et al., 1999; Corti et al., 2006). In fact, the extension of mixing presented in the previous subsection is still limited by the model layers and, consequently, is not suitable to parametrize unresolved convective events which connect the PBL with layers in the upper troposphere on a time scale of minutes to hours.

10   Now, we present an alternative method to enhance upward transport for conditionally unstable air parcels with $N_m^2 < 0$ in order to lift such air masses from the lowest layer of CLaMS $\Delta\zeta_{pbl}$ (following the orography and approximating here the PBL) into the upper troposphere. Figure 4 shows the concept of estimating the uplift of boundary air by adding a $\Delta\theta$ to the trajectory in the vertical direction when the condition $N_m^2 < 0$ is diagnosed along the trajectory.

Following Ertel (1938) (for details see appendix B), we use the following approximation for $\Delta\theta$:

15    $$\Delta\theta = \frac{L_v \theta_0 \mu_w}{c_p T}, \tag{3}$$
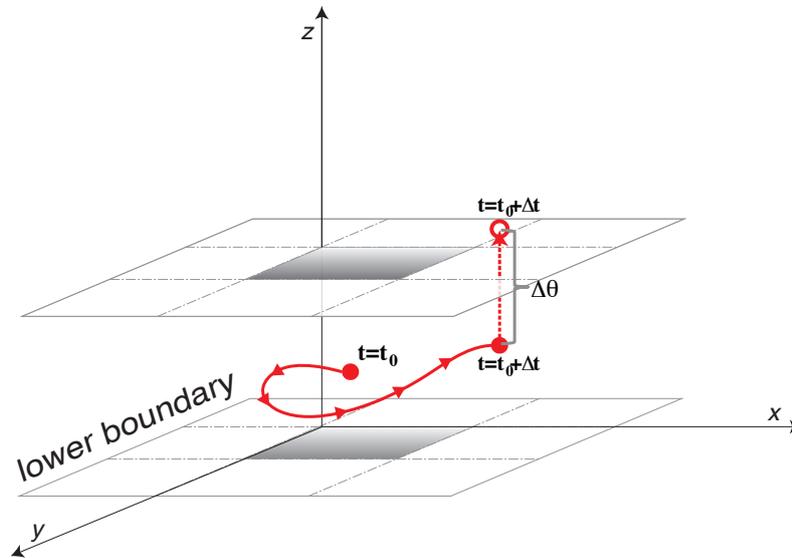
Figure 4. The original trajectory (thick solid red) and the modified trajectory (dashed red) with convective transport from the lowest CLaMS layer at time step $t_0 + \Delta t$. The vertical displacement $\Delta\theta$ of the considered air parcel is estimated through the latent heat release of condensation (see text for more details).

where θ_0 and μ_w denote the potential temperature and the total water vapor mass mixing ratio in the air parcel where the condition $N_m^2 < 0$ is fulfilled. L_v is the specific latent heat for evaporation and c_p denotes the specific heat at constant p.

To illustrate, how such a parametrization works, the zonally-resolved fraction of events with $N_m^2 < 0$ occurring within the lowest CLaMS layer are shown in Fig. 5. The respective DJF and JJA climatologies derived from ERA-Interim for 2005

5 reveal the expected spatial distribution, land-ocean contrasts as well as the seasonality. To justify the use of $N_m^2 < 0$ as a proxy of convection, we compare its spatial distribution with the satellite-based Outgoing Longwave Radiation (OLR, top row, cyan isolines) as well as with the ERA-Interim-based convective available potential energy (CAPE) as an alternative method to detect convection (for definition of CAPE, see appendix B). The comparison shows a good correlation between the climatology of the regions with $N_m^2 < 0$ and the respective OLR (top panel of Fig. 5) whereas the correlation with the

10 CAPE is less pronounced (e.g. in the region around 30-50E, 45°N during JJA). Motivated by this finding and because of the simplicity of tracing conditionally unstable air parcels, we use in the following the criterion $N_m^2 < 0$ as the first condition to trigger convective events.

Our second condition is related to the question if every conditionally unstable air parcel is a source of convection which should be taken into account. This question is also related to the fact that the number of air parcels in CLaMS is not strictly

15 conserved but kept roughly constant within about $\pm 10\%$ flexibility through the adaptive regridding procedure (current mixing
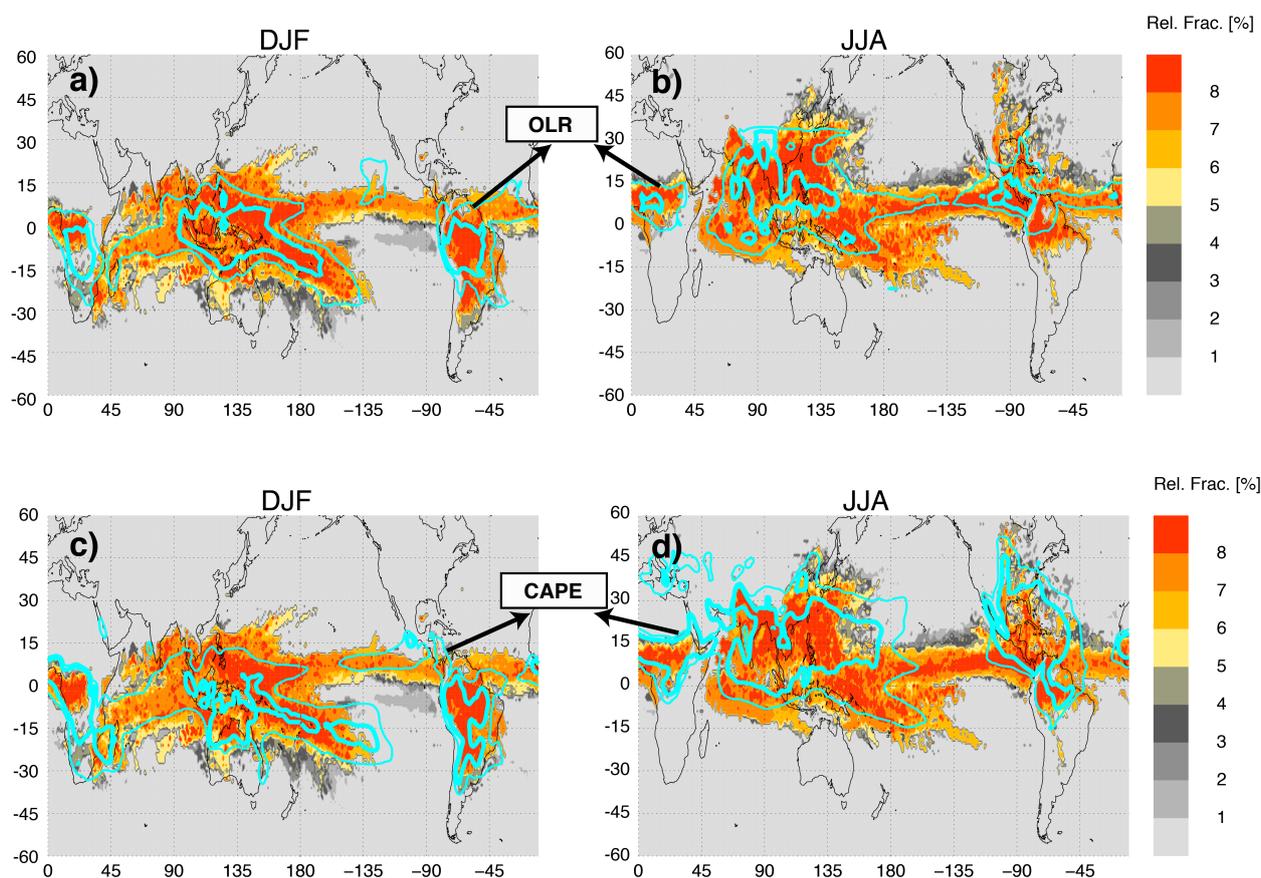
Figure 5. Color-coded is the fraction of ERA-Interim time steps (6h-frequency) within a season when the criterion triggering the deep convection scheme is fulfilled at CLaMS air parcels within the lowest layer of the model $\Delta\zeta_{pbl} = 250$K ($\sigma_r = 0.7$, for details see text). Left and right column show DJF and JJA 2005 climatologies, respectively. In the top row the isolines of the Outgoing Longwave Radiation (OLR) as derived from the NOAA satellite archive are highlighted while in the bottom row the isolines of the convective available potential energy (CAPE) are overplotted (cyan).
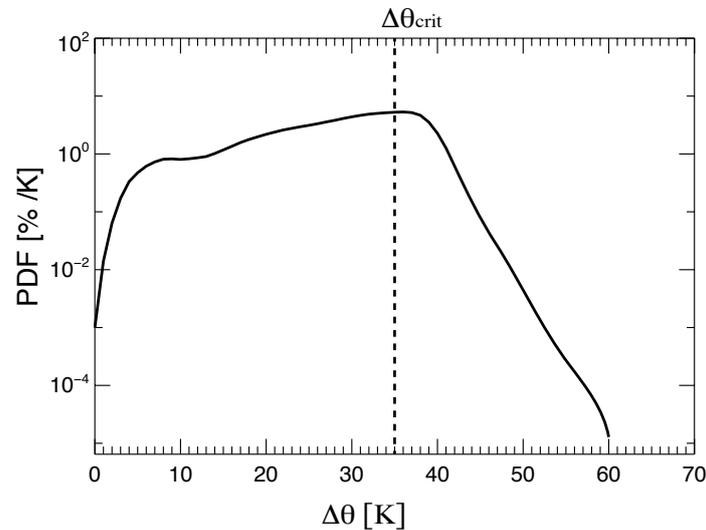
Figure 6. The probability distribution function (PDF, in units of %/K) of convective uplift $\Delta\theta$ in the tropics (30°S-30°N) for the air parcels in the lowest level of CLaMS ($\Delta\zeta = 250$ K, $\Delta z \approx 1.4 - 2$ km) where N_m^2 is negative using the ERA-interim reanalysis data of the year 2005. The restriction used for the "deep" convection scheme ($\Delta\theta > 35$ K) is marked as the dashed straight line.

scheme). It means that the mixing procedure is able to adjust a certain increase or decrease in the number of air parcels, but this amount should be below $\pm 10\%$. Figure 6 shows the one-year climatological PDF of $\Delta\theta$ in the tropics (30°S- 30°N). The probability of $\Delta\theta$ larger than 35 K is around 30% and it decreases rapidly from 35 K to 60 K. When the $\Delta\theta$ is too small to leave the lower boundary, it is not necessary to add $\Delta\theta$ to the trajectory. Thus, as our second condition, we only uplift such air parcel along the trajectory (i.e. within the advective step) if $\Delta\theta$ is sufficiently large. In our control runs, the minimum $\Delta\theta$ is set to 35 K shown as the dashed line in Fig. 6. This choice is also the reason that we call this parametrization "deep" convection scheme.

4   CLaMS performance with additional tropospheric transport

In this section, we describe the details of the CLaMS configuration for the runs with extended tropospheric transport, show in which part of the atmosphere the CLaMS air parcels are affected by this extension and compare the respective AoA distributions. Especially, we investigate the propagation of the CO_2 distribution from the boundary layer into the lower stratosphere for different model configurations and validate the related CO_2 variability (annual cycle and trend) with the observations and the CarbonTracker model simulations.

4.1 Setup for control runs

Like for the reference run described in the subsection 3.1, the runs with extended tropospheric transport (in the following denoted as control runs) cover the same time period 2005-2008 and have the same vertical and horizontal resolution above the tropopause. To resolve the diurnal cycle of our new parametrization, we decrease the advective time step of trajectories from 24 to 6 hours and, to keep the intensity of the standard CLaMS mixing scheme roughly constant, we also increase the Lyapunov

5 exponent from 1.5 to 3.5 day^{-1} corresponding to the critical deformation $\gamma_c = 0.85$. Such a slightly higher mixing frequency relative to the reference case (every 6 instead of every 24 hours) has proven to give better representation of the CO-ozone correlations in the UTLS region (Vogel et al., 2011; Konopka and Pan, 2012).

For CLaMS control runs, we also use two slightly different grid configurations: $\sigma_r = 0.7$, $\Delta\zeta_{pbl} = 250$K (Fig. 7b) and $\sigma_r = 0.3$, $\Delta\zeta_{pbl} = 140$K (Fig. 7c). Grid configurations for the reference run ($\sigma_r = 0.3$, $\Delta\zeta_{pbl} = 100$K) and the control runs

10 are the same in the stratosphere although significant differences are in the troposphere: By using $\sigma_r = 0.7$, isentropic mixing and diabatic vertical velocities, two central concepts of CLaMS, can be extended to a larger part of the troposphere, in particular to the middle tropical troposphere. Note that the 320, 330K isentropes in the left bottom panel of Fig. 7) are within CLaMS layers defined by the ζ coordinate and, consequently, mixing within such layers is roughly isentropic. Consequently, almost the whole UTLS region, down to the tropical middle troposphere, is covered by such isentropic layers in the $\sigma_r = 0.7$ simulation

15 (see Tao et al. (2018), especially their appendix 1).

Furthermore, both apparently different choices of $\Delta\zeta_{pbl}$ ($\sigma_r = 0.7/0.3$) for the control runs correspond roughly to the same geometric thickness of the lowest CLaMS layer, which varies between 1.4 and 2.2 km and approximates here the PBL. It should be emphasized that by using pre-defined boundary conditions in the PBL, we do not resolve any transport in this part of the atmosphere and confine our efforts only to improve transport in the free troposphere extending between the PBL and

20 the tropopause. In order to be conform with the standard model version described in section 3.1 (Pommrich et al., 2014), $\Delta\zeta_{pbl} = 100$K is used in the reference run.

Figure 7 shows the zonal mean distribution of the mean age of air (AoA), calculated relative to the Earth's surface for one day (19.08.2005) and plotted for the three cases discused above: reference run with $\sigma_r = 0.3$, $\Delta\zeta_{pbl} = 100$K (Fig. 7a) and two control runs with extended tropospheric transport (FULL_EXT): $\sigma_r = 0.7$, $\Delta\zeta_{pbl} = 250$K (Fig. 7b) and $\sigma_r = 0.3$, $\Delta\zeta_{pbl} = 140$K (Fig. 7c). Both types of control runs show much younger air in the troposphere if compared with the reference run. Also the gradients across the tropopause are more pronounced. On the other hand, stratospheric distributions are very similar for all three cases. Table 1 provides the key information for all CLaMS reference and control runs discussed in this paper.

4.2 Diagnostic of extended tropospheric transport

It is easy to tag and count all air parcels in CLaMS which undergo additional tropospheric mixing and which are lifted from the lower boundary to the middle and upper troposphere by the deep-convection scheme introduced in the previous section. In Fig. 8a/b the DJF/JJA zonally averaged fractions of additionally mixed air parcels (calculated for 2005) are color coded as
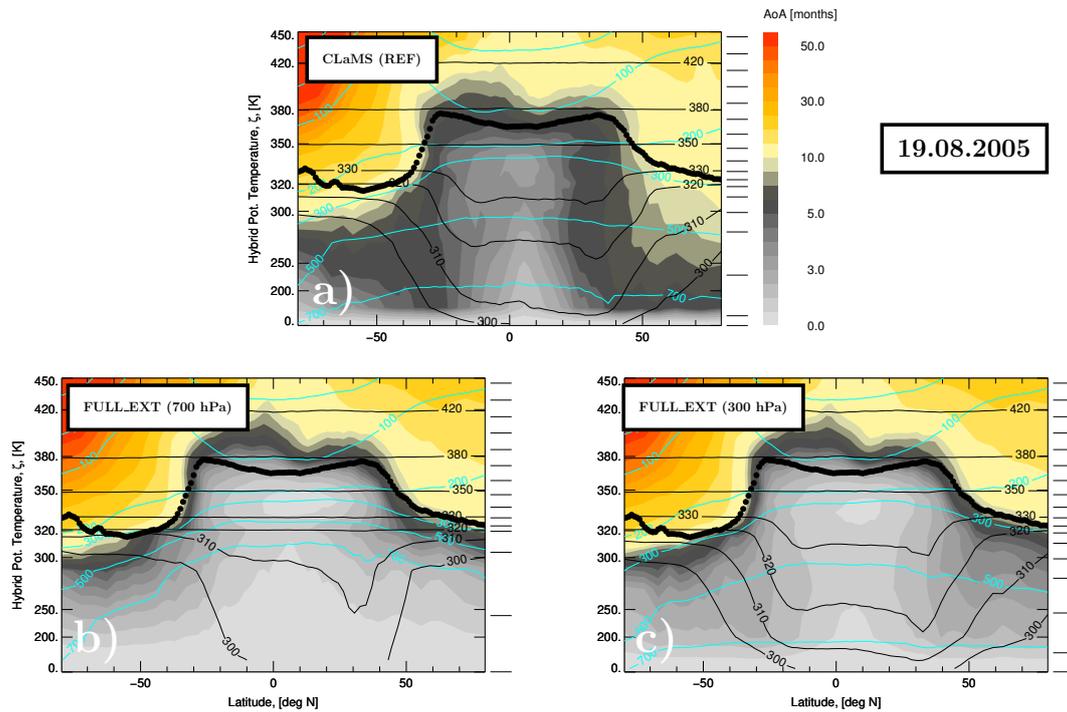
Figure 7. Zonal mean of mean age (AoA) for the reference run (a) and for the runs with tropospheric mixing (bottom) exemplarily calculated for 19.08.2005 (i.e. after more than 8 months of transport). In the bottom panel, two configurations for $\sigma_r = 0.7$ (b) and 0.3 (c) are shown. The hybrid vertical coordinate ζ is used and the isolines of the potential temperature θ (black), pressure p (cyan) as well as the zonal mean of the WMO tropopause are also shown. On the right side of each panel, the boundaries of the used layers are plotted (see text for more details).

Table 1. List of CLaMS reference and control runs with different configurations of mixing parametrization and convective transport.

Name	time step	λ_c day^{-1}	unresolved convection	tropospheric mixing	σ_r
REF	24 hr	1.5	N	N	0.3
REF − 6H	6 hr	3.5	N	N	0.7
TROP_MIX	6 hr	3.5	N	Y	0.7
UNRES_CONV	6 hr	3.5	Y	N	0.7
FULL_EXT	6 hr	3.5	Y	Y	0.7
FULL_EXT	6 hr	3.5	Y	Y	0.3
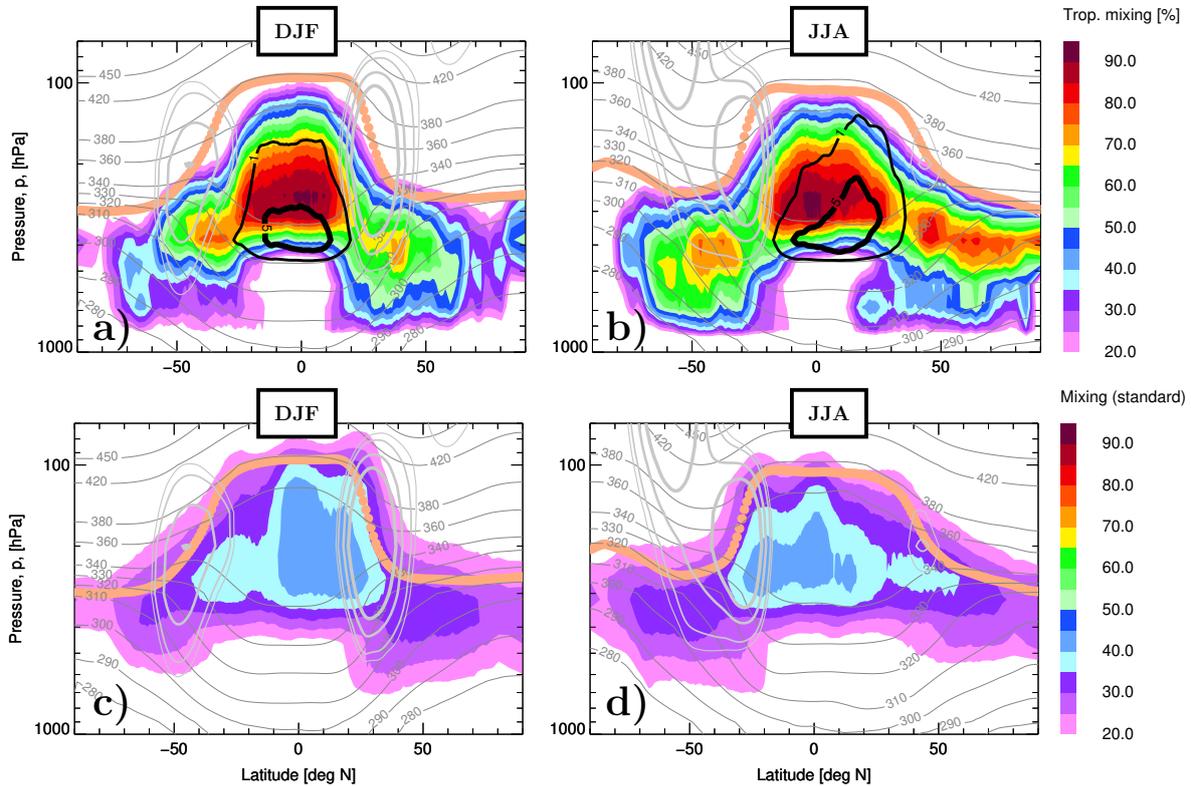
Figure 8. Top: DJF/JJA 1-year (2005) climatology of percentage of CLaMS air parcels undergoing tropospheric mixing (colors) and of air parcels lifted from the lowest layer of the model into the middle and upper (tropical) troposphere (black contours). Bottom: Same type of climatology but for air parcels which undergo the standard CLaMS mixing procedure (adaptive regridding driven by horizontal strain and vertical shear within the CLaMS layers). The respective WMO tropopause (beige), horizontal wind marking the position of the jets (light gray) and the isentropes (dark gray) are also shown.

the function of latitude and pressure. The black isolines in the top panel approximate the fraction of the CLaMS air parcels which were lifted from the lowest boundary layer to the middle and upper tropical troposphere using the deep convection parametrization. For comparison, the fractions of the number of air parcels affected by the default CLaMS mixing scheme are shown in the bottom panels of Fig. 8, which always happens, independent if the here discussed extension of transport is included or not. In addition, the respective mean WMO tropopause as well as the isentropes are shown.

Note that the tropopause separates well the troposphere from the stratosphere where CLaMS tropospheric mixing practically does not affect any air parcels (the zero line of the calculated fraction is well below the tropopause, not shown). Note also that numbers of air parcels affected by the deep convection scheme are smaller than 10% with highest levels (around 360 K) during JJA, mainly related to the Asian Summer Monsoon (not shown). Furthermore, both tropospheric mixing and the deep convection transport show some seasonality like N^2 and N_m^2, respectively (i.e. higher in the summer hemisphere). Finally, the default mixing scheme is much weaker than the tropospheric mixing although the seasonality is very similar. Note that this

part of mixing is also present in the vicinity of the tropopause although with stronger signatures on the tropical side of the jets

10 and below the tropopause. At least in this climatological picture, only standard mixing in CLaMS contributes to a direct STE.

4.3 Validation with CO_2 observations

CO_2 is a useful tracer for validation of transport in the models, mainly in the troposphere and lower stratosphere where CO_2 is basically chemically inert (Waugh and Hall, 2002). The only stratospheric source of CO_2 is a small contribution ($<$1 ppmv) from methane oxidation (Boucher et al., 2009) that is taken into account in all CLaMS simulations discussed here (Pommrich

5 et al., 2014). Thus, the quality of the CO_2 distribution reproduced in CLaMS is determined largely by the quality of the lower boundary condition and the quality of the representation of transport. For the latter, tropospheric transport, is a significant part.

The atmospheric mixing ratios of CO_2 are essentially both monotonically increasing (trend) and periodic (seasonality) signals which define a stringent test for the model representation of tropospheric transport and STE (Bönisch et al., 2008, 2009). As recently shown by Diallo et al. (2017), even inverted vertical profiles of CO_2 across the extratropical tropopause

10 are possible during the Northern Hemispheric summer despite of a continuous increase of the mean CO_2 in the PBL resulting from the growing anthropogenic emissions.

In CLaMS, CO_2 mixing ratios propagate upwards from the lowest layer $\Delta\zeta_{pbl}$ for which the CarbonTracker data set was used (Peters et al. (2007), the updates are documented at http://carbontracker.noaa.gov) with CO_2 mixing ratios available for the 2000-12 period (run CT2013B, available every 3 hours, see ftp:/products/carbontracker/co2/CT2013B/molefractions/co2_total/).

15 In particular, the first five lowest levels of each CarbonTracker data set were vertically averaged and used to overwrite CLaMS air parcels within the PBL layer every 6 hours. The reference run was initialized at 01.01.2000 and beginning from 01.01.2005 all other control runs were started using the output of the reference run for the initial distribution.

The zonal means of CO_2, exemplarily calculated for two representative days, 5th of Mai and 25th of September, 2005, are shown in Fig. 9. In particular, results for the reference run (REF) and for the two control runs with full tropospheric transport

20 (FULL_EXT, $\sigma_r = 0.3/0.7$) can be compared with the respective CarbonTracker distribution which was used in CLaMS to intialize the lower boundary of the model. In all CO_2 distributions, the upward propagation of the annual cycle can be clearly diagnosed with higher values during the boreal summer and vertical inversion during the fall. However, the propagation of the tropospheric signal shows some obvious differences with a faster upward propagation in CLaMS control runs than in the CLaMS reference run. Note that the cross-hemispheric transport is weaker in the $\sigma_r = 0.7$ than in the $\sigma_r = 0.3$ CLaMS

25 configuration, the former being in better agreement with CarbonTracker. Note also that the upward propagation of the CO_2 annual cycle is well-confined by the position of the tropopause (black dots) in all CLaMS runs while in the CarbonTracker data this property is less pronounced, although like in CLaMS, ERA-Interim reanalysis is used to run the underlying transport model (see CT2013B documantation: https://www.esrl.noaa.gov/gmd/ccgg/carbontracker/CT2013B). We will come to this point later.

Now, the CO_2 time-space evolution derived from such CLaMS simulations are compared with the observations of the Com-

30 prehensive Observation Network for TRace gases by AIrLiner (CONTRAIL) (Machida et al., 2008). CO_2 mixing ratios were measured during regular flights by Japan Airlines from Japan to Australia, Europe, North America, and Asia with continuous measuring equipment (CME) for in situ CO_2 observations, as well as improved automatic air sampling equipment (ASE) for
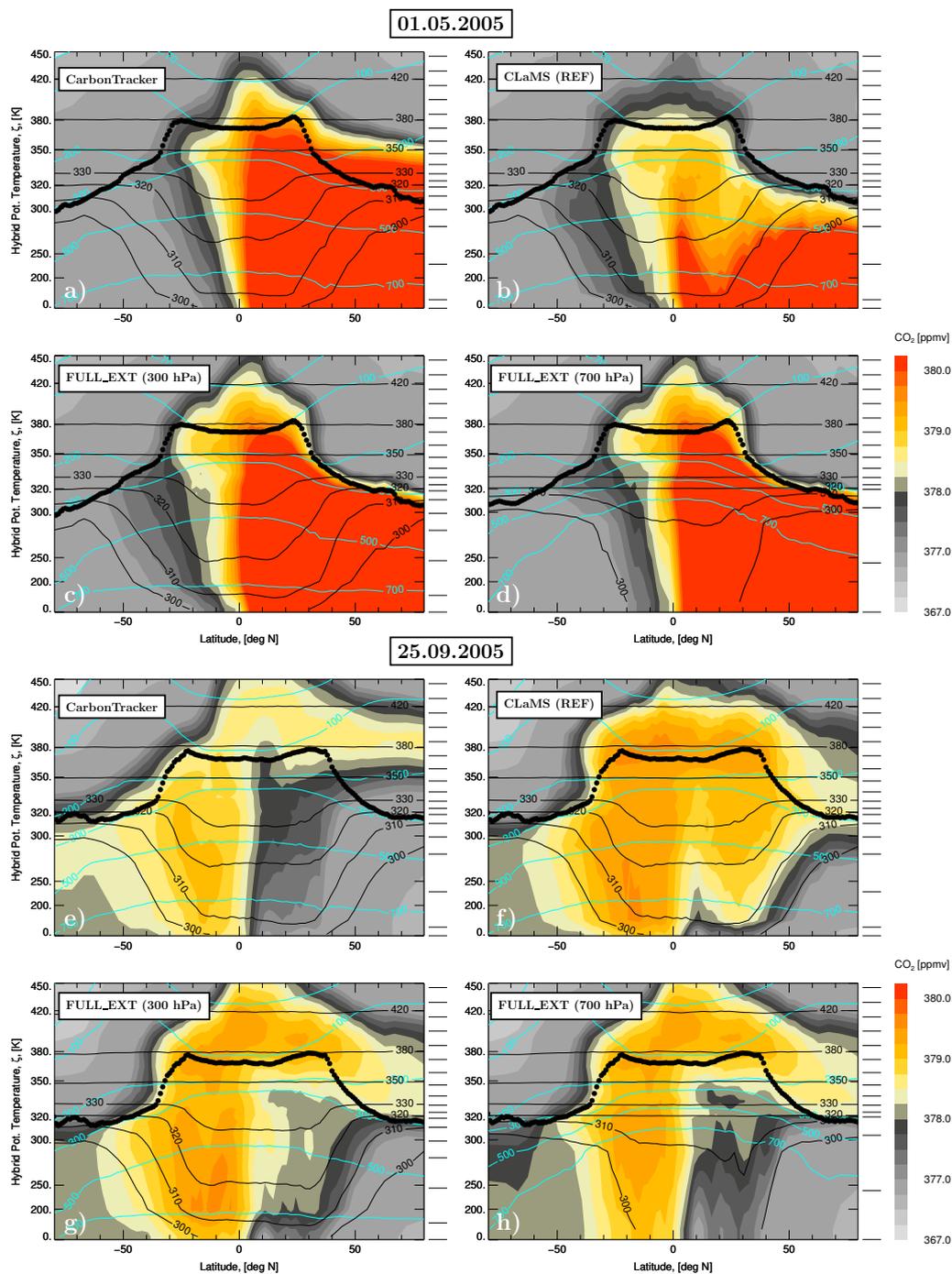
Figure 9. Upward propagation of the CO_2 distribution from the lowest layer of the model where CO_2 was initialized by the CarbonTracker data (CT2013B) on two exemplary days: 01.05.2005 (a to d) and 05.09.2005 (e to h). The CLaMS zonal means for different model configurations are compared with the CarbonTracker distribution itself. Black dots denote the tropopause derived from the ERA-Interim data.
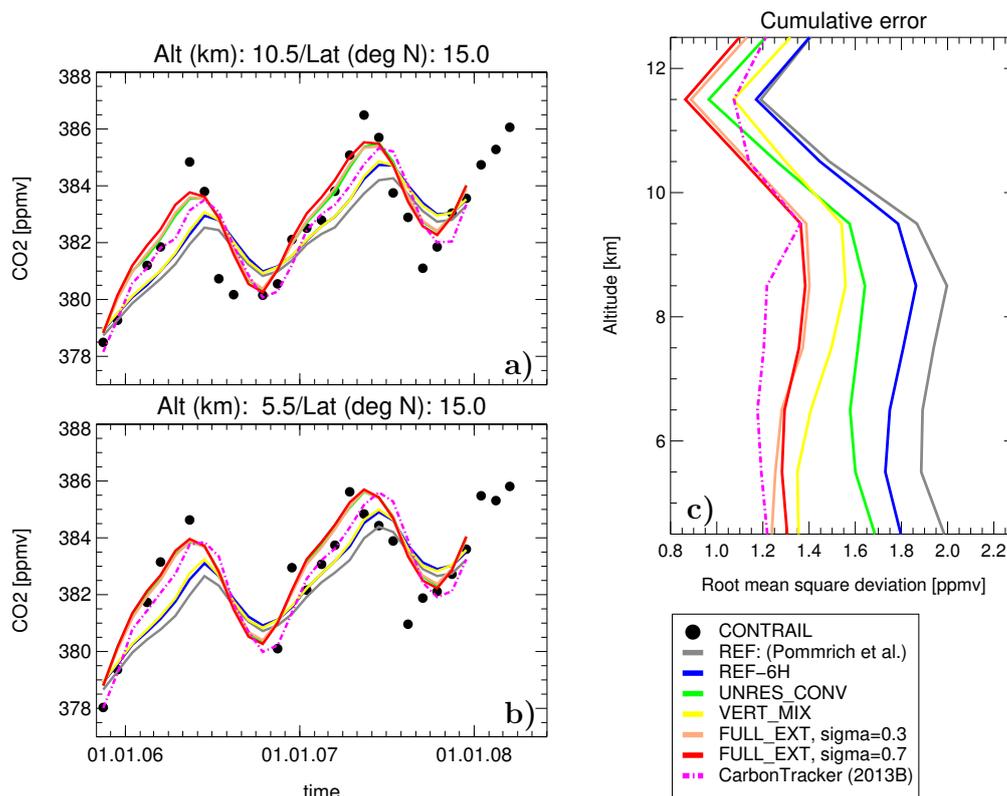
Figure 10. Left: Seasonality of CO_2 for CLaMS runs compared with CONTRAIL observations (black filled circles) at two locations: $15°N$, 5.5 km (a) and $15°N$, 15.5 km (b) Right: The accumulated errors of CO_2 for CLaMS runs compared with the CONTRAIL observations as the function of the altitude.

flask sampling (for more details about the instrument see Machida et al. (2002)). This data set provides significant spatial coverage, particularly in the Northern Hemisphere (Sawa et al., 2015). CONTRAIL observations have a vertical resolution of a few meters (during ascents and descents) and a horizontal resolution of a few hundred meters, resulting from the high sampling frequency of these instruments.

Here, we use the zonally and monthly averaged time evolution of these observations between 2005 and 2008 interpolated at a latitude-altitude grid with $10° \times 1$ km resolution and extending between $20°S$ to $60°N$ and 5.5-12.5 km, respectively (for more details see Diallo et al. (2017)). Comparison of these mean CONTRAIL observations with the respective CLaMS results for the reference and all control runs are shown in Fig. 10.

In particular, the comparison of the seasonal cycle and trend at $15°N$ for two selected altitudes of 5.5 and 10.5 km is plotted in the left panel of Fig. 10. The right panel shows the accumulated error, i.e. the zonal mean of the mean square deviation between the CLaMS simulation and CONTRAIL observations averaged over all latitude-altitude grid points where gridded

10 (mean) measurements are available. Thus, the reference run (REF) and the run with 6h mixing frequency (REF-6H) show not only too small amplitude but also their phase is delayed if compared with the CONTRAIL observations.

There is a clear improvement of the representation of the CO_2 distribution quantified in terms of the phase and the amplitude of the seasonal cycle as well as in terms of the accumulated error by taking additional tropospheric transport into account. The best results are achieved by including both the tropospheric mixing and the convection parametrization (orange and red curves are for $\sigma_r = 0.3$ and 0.7, respectively). By switching off the tropospheric mixing or the convection parametrization or both (here the results only for $\sigma_r = 0.7$ are shown), the cumulative error increases up to 80%. While the tropospheric mixing is

5 more important below 9 km, the improvement due to convection parametrization dominates between 9 and 13 km. Also there are still some errors in the amplitude, the additional tropospheric mixing significantly improves the overall agreement. Note that also the CarbonTracker distribution, even achieved by assimilating observations does not show a perfect comparison with the CONTRAIL observations (which are not included into the assimilation procedure of the here used version CT2013B). Remarkable, CLaMS control simulations are beccoming even better than CarbonTracker distributions in the region above

10 10 km probably caused by a very limited vertical resolution of the CarbonTracker data around the tropopause (only 6 levels between 9 and 18 km).

4.4 Impacts on the stratosphere

For this purpose, we discuss the differences in the distribution of AoA due to extension of tropospheric transport by considering its annual and zonal mean calculated for the year 2007 (last year of our simulations covering the 2005-07 period) and shown in Fig. 11. We compare our reference CLaMS run (i.e. based on the standard CLaMS configuration described Pommrich et al. (2014), top panel) with two control runs containing the full extension of tropospheric transport, but different configurations of

5 the CLaMS default mixing scheme (Fig. 11b and c). From the left to the right bottom panel, the default mixing intensity was reduced by increasing λ_c from 3.5 to 4.0 day^{-1}.

As expected, the comparison of these two runs with the reference shows that the air below the tropical tropopause becomes younger by up to 6 month if the additional tropospheric transport is included. However, and at first surprisingly, the air becomes slightly older in the stratoshere, by around 12% (not shown) and up to 6 month in the polar stratosphere.

10 Note that this is not a consequence of enhanced tropospheric transport but of the change in the default mixing scheme from $\Delta t = 24$ hours, $\lambda_c = 1.5$ day^{-1} (reference) to $\Delta t = 6$ hours, $\lambda_c = 3.5$ day^{-1} (control, left bottom panel). Such a change leads to a slightly enhanced isentropic mixing across the tropical pipe, which also enhances the stratospheric re-circulation and makes the stratospheric air older due to aging by mixing (Garny et al., 2014; Poshyvailo et al., 2018). Consistently with the hemispheric asymmetry of eddy mixing, the effect of aging by mixing is slightly larger in the Northern than in the Southern

15 Hemisphere (not shown).

Furthermore, aging by mixing becomes smaller by reducing the isentropic part of CLaMS mixing (by setting $\Delta t = 6$ hours, $\lambda_c = 4.0$ day^{-1} in the default mixing scheme, right bottom panel in Fig. 11) although the tropospheric AoA is almost the same as for the control run. This indicates a secondary role of CLaMS standard mixing scheme in the troposphere and underlines
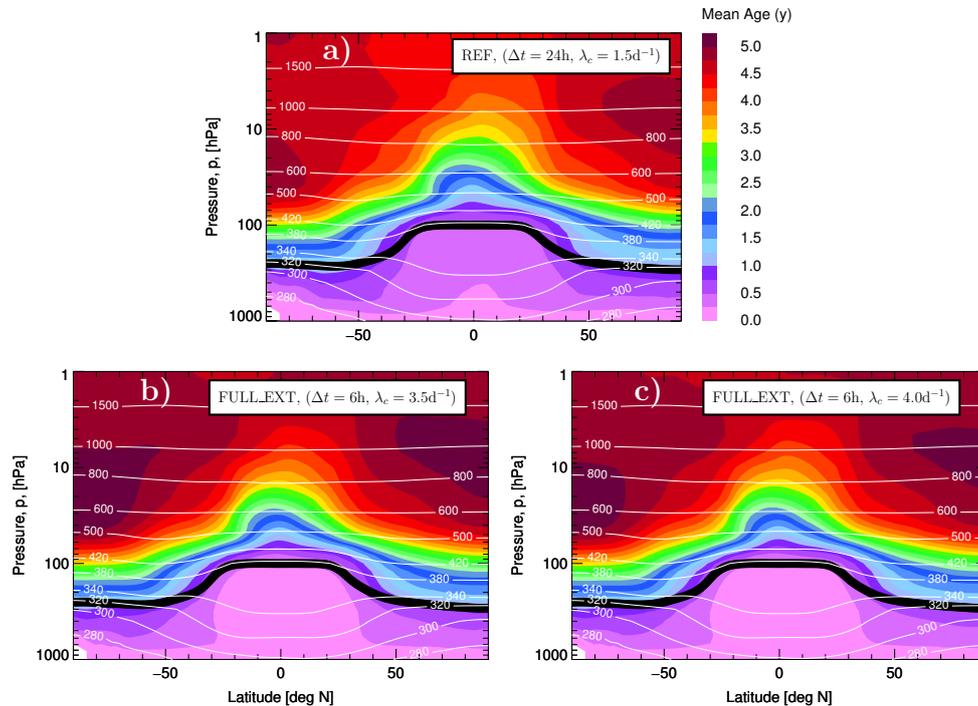
Figure 11. Annual and zonal mean of AoA (for 2007) as derived from the reference run (a) and from two control runs with new tropospheric transport (FULL_EXT) but for two different configurations of the standard CLaMS mixing scheme (b and c). Black line denotes the tropopause.

its primary role in the stratosphere. In this way, the cross-tropopause gradient of AoA can be enhanced by combining the
20   stratospheric mixing with the proposed extension of tropospheric transport.

5   Conclusions

Implementation of mixing in Lagrangian transport models is still an important issue in the ongoing scientific discussion. Here, we follow the idea of using numerical diffusion to parametrize physical mixing which was first proposed and inplemented in connection with the Chemical Lagrangian Model of the Stratosphere (CLaMS). In particular, we extend this idea to the tropo-
25   sphere where vertical stability is much smaller if compared with the stratosphere for which CLaMS was originally developed. By using the lapse rates of the dry and moist potential temperature mainly defining the squares of the dry and moist Brunt Vaisaila frequencies N^2 and N_m^2, we parametrize two important troposheric processes which are not sufficiently resolved in the current version of CLaMS Pommrich et al. (2014), i.e.: subgrid tropospheric mixing in regions with small lapse rates of the dry potential temperature and unresolved (deep) convection in regions with conditionally unstable lapse rates of the moist
30   potential temperature.

The implementation of both processes improves CLaMS performance measured here in terms of the quality of the simulated CO_2 seasonality. However, there is still some freedom in the choice of the free parameters and in the representation of the PBL in the model. By including other species like CO, ozone, CH_4 and water vapor and comparing such distributions with observations, we plan in the future to reduce these degrees of freedom. On the other hand, by covering the whole range of possible variability of tropospheric transport, we will be also able to find the respective variability of the air composition

5 entering the stratopshere, especially the effects on the stratospheric water vapor.

Appendix A: Vertical instability, Brunt Vaisala frequency and convective available potential energy (CAPE)

Vertical instability is strongly related to the concept of buoyancy. We condense now some textbook knowledge and start from the Boussinesq approximation of the vertical momentum equation by taking into account only buoyancy effects (see e.g. Salby (1996) or Vallis (2006)), i.e.:

$$\frac{Dw}{Dt} = -\frac{1}{\rho_0}\frac{\partial \Delta p}{\partial z} - g\frac{\Delta\rho}{\rho_0} \approx -g\frac{\Delta\rho}{\rho_0}. \tag{A1}$$

The solution of this equation describes the vertical velocity w of an air parcel in a hydrostatic reference atmosphere, i.e. defined by the relation $\partial_z p_0 = -\rho_0 g$ with mean pressure and air mass denisty profiles given by $p_0(z)$ and $\rho_0(z)$, respectivelly (z - geometric altitude, g - gravity of Earth). The Δ-quantities, i.e., Δp and $\Delta\rho$ describe the deviation from such a mean state.

The right hand side of eq. (A1) quantifies the buoyancy. Following Archimedes, the mass-related buoyancy F_b/m can be

15 derived from the weight of the environmental fluid replaced by the parcel, i.e.

$$-\frac{F_b}{m} = \frac{\rho g V - \rho_0 g V}{\rho V} = g\frac{\rho - \rho_0}{\rho} \overset{\text{Boussinesq}}{=} g\frac{\rho - \rho_0}{\rho_0} = g\frac{\Delta\rho}{\rho_0}, \tag{A2}$$

where, using the Boussinesq approximation, ρ was replaced by ρ_0. With $w = \Delta z/dt$ and $\Delta\rho = -(d\rho_0/dz)\Delta z$, the following equation for Δz can be derived:

$$\frac{d^2}{dt^2}\Delta z + N^2\Delta z = 0, \quad N^2 = -\frac{g}{\rho_0}\frac{d\rho_0}{dz}, \tag{A3}$$

20 with N denoting the Brunt-Vaisala frequency. Using the ideal gas law and assuming the incompressibility of the flow, we get (for details see e.g. Vallis (2006)):

$$\frac{\Delta\rho}{\rho_0} = -\frac{\Delta\theta}{\theta_0}. \tag{A4}$$

With $\Delta\rho = -\Delta\theta\,(\rho_0/\theta_0) = -(\rho_0/\theta_0)(d\theta_0/dz)\Delta z$, the Brunt-Vaisala frequency can be also rewritten to the well-known definition (index "o" is omitted):

$$N^2 = \frac{g}{\theta}\frac{d\theta}{dz}. \tag{A5}$$

In general, eq. (A3) has two types of solutions: periodic (i.e. stable) solutions for $N^2 > 0$ and exponentially increasing (i.e. unstable) solutions for $N^2 < 0$. We conclude that the lapse rate of the potential temerature θ defines the stability and the instability
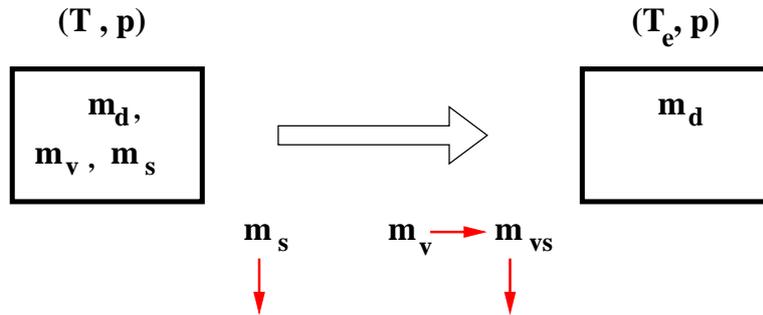
Figure A1. The equivalent potential temperature T_e of an air parcel with temperature T and pressure p and with the dry mass m_d, water vapor content m_v and the liquid/solid water content m_s. T_e is defined by a reversible process completely removing m_v by vapor-water condensation (i.e. transforming pseudoadiabatically m_v into m_{vs}) and by using this energy to heat the original air parcel by $p = $ const, i.e. $T_e > T$. Liquid and/or solid water (m_s) are removed. but without any correction of T_e. (i.e. due to sedimentation this is a pseudoadiabatic and not a pure adiabatic process).

of the atmospheric environment through the positive and negative lapse rate $d\theta/dz$ (or through the positive and negative values of N^2), respectively.

30   Now, we generalize this concept to the atmosphere containing water vapor, i.e. to the moist atmosphere (see e.g. Salby (1996)). First, we define the equivalent potential temperature θ_e by using the equivalent temperature, i.e. the temperature of an air parcel from which all the water vapor has been extracted by an adiabatic process (see also Fig. A1):

$$\theta_e = \frac{T_e}{T}\theta \; , \qquad T_e = T + \frac{L}{c_p}\mu_w \; . \tag{A6}$$

L is the latent heat of evaporation and μ_w the water vapor mixing ratio. The energy released by the phase transition from

5   liquid water to the ice phase can be neglected in most cases because the respective latent heat is smaller by a factor of 10 than the latent heat of gas-liquid transition (334 kJ for melting versus 2270 kJ for evaporation for 1 kg liquid water). There is a number of different defintions of the equivalent potential temperature (Bolton, 1980). Our defintion corresponds to the simplified formula proposed by Stull (1988).

Using the same type of arguments as for the dry atmosphere, we also quantify the vertical instability of the moist atmosphere

10   in terms of the lapse rate of the equivalent potential temperature θ_e or in terms of the respective (moist) Brunt Vaisala Frequency N_m, i.e.

$$N_m^2 = \frac{g}{\theta_e}\frac{d\theta_e}{dz} \; . \tag{A7}$$

However, atmospheric environments with a negative lapse rate of the equivalent potential temperature or with negative values of N_m^2 define only the so-called conditionally unstable atmosphere (see e.g. Salby (1996)), i.e. regions which could be unstable

15   if the respective phase transition releasing latent heat would happen (such air parcels with $N_m^2 < 0$ are not necessarily saturated, so some unresolved motions like adiabatic gravity waves are needed to get saturation).
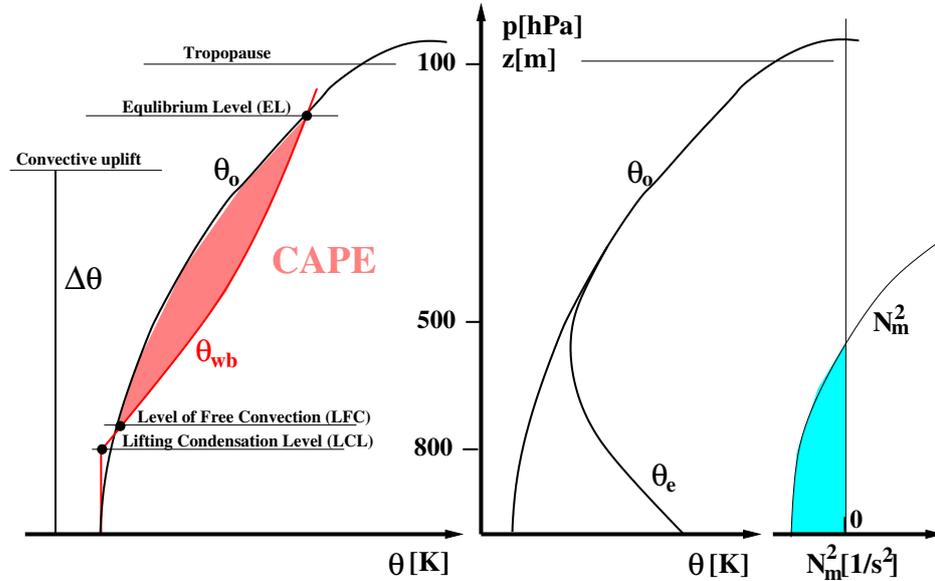
Figure A2. CAPE (red) versus stability-based (cyan) measure of potential convective uplift $\Delta\theta$ transporting CLaMS air parcels from the PBL to the upper troposphere. For more explanation see text.

For comparison, we also use the known concept of convective available potential energy (CAPE) which can be undestood as a different measure of the unstable buoyancy (Emanuel, 1994). Starting form (A2) and (A4), we can write:

$$-\frac{F_b}{m} = g\frac{\rho - \rho_0}{\rho_0} = -g\frac{\theta - \theta_0}{\theta_0} \tag{A8}$$

Then, CAPE is defined as the following integral (in J/kg, see also Fig. A2):

$$5 \quad \text{CAPE} = \int_{z_{min}}^{z_{max}} \text{``unstable buoyancy force''} \, dz = \int_{\text{LFC}}^{\text{EL}} g\frac{\theta_{wb}(z) - \theta_0(z)}{\theta_0(z)} \, dz. \tag{A9}$$

Whereas $\theta_0(z)$ is the dry potential temperature of the environment (ambient air), $\theta_{wb}(z)$ is the so-called wet-bulb potential temperature which needs some further explanations: We begin with the lifting condensation level (LCL) defined as the height at which a parcel of air becomes saturated when it is lifted adiabatically from the Earth's surface (so the potential temperature does not change). Starting from the LCL the air parcel is than transported along a moist adiabat (also known as saturation-adiabatic process, i.e. an pseudoadiabatic process for which the air is saturated). The corresponding dry potential temperature within such a parcel defines the wet-bulb potential temperature. Note that a distinction is made between the reversible process, in which total water is conserved, and the pseudoadiabatic or irreversible moist adiabatic process, in which liquid water is assumed to be removed as soon as it is condensed (see also Fig. A1). The cross points of such a moist adiabate with $\theta_0(z)$

define the region with unstable conditions (red). The lowest cross point defines the level of free convection (LFC) whereas the equilibrium level (EL) is the height where the (potential) temperature of a buoyantly rising parcel again equals the (potential) temperature of the environment.

In this paper, we use the condition $N_m^2 < 0$ rather than condition CAPE > 0 to find those air parcels in the lowest model level (approximating the PBL) which might undergo convection (see Fig. A2). In the next appendix, we discuss an additional
5 assumption quantifying the vertical displacement of such air parcels.

Appendix B: Latent heat release versus vertical transport

To derive the expression (B7) quantifying the convection-driven vertical uplift $\Delta\theta$ from the latent heat δQ available within the air parcel, we assume that the source of heating is only the latent heat release of water vapor condensation. For a unit mass, we get along a moist adiabate (see e.g. Salby (1996)):

10 $$\delta Q = -L_v d\mu_s \tag{B1}$$

where L_v is the specific latent heat for water evaporation (or condensation) and μ_s is the saturation water vapor mass mixing ratio.

Using the entropy definition of the potential temperature $\theta := \theta_0 \exp(s/c_p)$ with s being the specific entropy measured in J/(K kg), c_p denoting the specific heat at constant p and θ_0 being the temperature T_0 that the air parcel would acquire if
15 adiabatically brought to the surface pressure p_0, we get:

$$ds = c_p \frac{d\theta}{\theta}. \tag{B2}$$

Thus, using the second low of thermodynamics, $ds = \delta Q/T$ and substituted δQ by the relation (B1), $d\theta$ can be derived as

$$d\theta = -\frac{L_v \theta d\mu_s}{c_p T}, \tag{B3}$$

where T is the saturation temperature. Then, we integrate from the initial state θ_0 to the state $\theta_0 + \Delta\theta$ when certain amount of
20 water vapor $\Delta\mu_s$ is condensed:

$$\int_{\theta_0}^{\theta_0 + \Delta\theta} \frac{d\theta}{\theta} = -\int_{\mu_s(\theta_0)}^{\mu_s(\theta_0+\Delta\theta)} \frac{L_v d\mu_s}{c_p T}. \tag{B4}$$

The result of the integral can be written as:

$$\Delta\theta = \theta_0 [\exp\left(\frac{L_v \Delta\mu_s}{c_p T}\right) - 1], \tag{B5}$$

where $\Delta\mu_s = \mu_s(\theta_0) - \mu_s(\theta_0 + \Delta\theta)$. Because $\frac{L_v \Delta\mu_s}{c_p T} \ll 1$, a first order approximation of the right hand side of eq. (B5) through
25 the Taylor expansion of the exponential function (Ertel, 1938) is

$$\Delta\theta = \frac{L_v \theta_0 \Delta\mu_s}{c_p T}, \tag{B6}$$

which gives a relationship between the total change of the potential temperature and the change of water vapor mass mixing ratio. Strictly, $\Delta\mu_s$ is the change of the water vapor saturation mass mixing ratio before and after a model time step. In our "deep convection" scheme, $\Delta\mu_s$ is estimated by the total water vapor mass mixing ratio μ_w before the model time step with the assumption that 1) the time scale of deep convection and its associated condensation is smaller than one model time step (here:

5 6 hours), 2) the residual water vapor content after deep convection ($\mu_s(\theta_0 + \Delta\theta)$) is so small that it can be neglected. Thus, the $\Delta\mu_s$ is assumed to be the total water vapor mass mixing ratio μ_w in the air parcel within the lowest layer of CLaMS where the criterion ($N_m^2 < 0$) is fulfilled. Therefore, the uplifting of an air parcels in our "deep convection" scheme is estimated by

$$\Delta\theta = \frac{L_v\theta_0\mu_w}{c_pT}. \tag{B7}$$

Acknowledgements. The European Centre for Medium-Range Weather Forecasts (ECMWF) provided meteorological analysis for this study.

10 We thank to the CONTRAIL team, in particular to Toshinobu Machida and Yousuke Sawa for helping us to use this data set. The authors sincerely thank Andy Jacobson and Pieter Tans from NOAA for support related to the CarbonTracker data. We also thank Rolf Müller and Michael Volk for helpful discussions. We are thankful to Marta Abalos for providing us with the WACCM e90 climatology. Excellent programming support was provided by N. Thomas. This research was supported by the German Helmholtz-Gemeinschaft within the Helmholtz-CAS joint research group (JRG) "Climatological impact of increasing anthropogenic emissions over Asia".

Code and data availability. The CLaMS code as used in Pommrich et al. (2014) is now implemented into the Modular Earth Submodel

5 System (MESSy) system (Version 2.53, https://www.messy-interface.org/). The here described extension will be included into the one of next releases of MESSy and until then this code can be requested from the corresponding author (p.konopka@fz-juelich.de) or can be found in the supplement. The CONTRAIL CO_2 data are openly accessible (doi:10.17595/20180208.001). The CarbonTracker data (version 2013B) can be downloaded from ftp:/products/carbontracker/co2/CT2013B/molefractions/co2_total/. For more detailed model data, please contact the authors.

References

Abalos, M., Randel, W. J., Kinnison, D., and Garcia, R.: Using the artificial tracer e90 to examine present and future UTLS tracer transport in WACCM, J. Geophys. Res., 74, https://doi.org/10.1029/2002JD002634, 2017.

Balsley, B. B., Svensson, G., and Tjernström, M.: On the Scale-dependence of the Gradient Richardson Number in the Residual Layer, Boundary-Layer Meteorol., 72, 57:72, https://doi.org/10.1007/s10546-007-9251-0, 2008.

Bolton, D.: The Computation of Equivalent Potential Temperature. Mon. Wea. Rev., Mon. Wea. Rev., 108, 1046–1053, 1980.

Bönisch, H., Hoor, P., Gurk, C., Feng, W., and Chipperfield, M.: Model evaluation of CO_2 and SF_6 in the extratropical UT/LS region, J. Geophys. Res., D06101, https://doi.org/10.1029/2007JD008829, 2008.

Bönisch, H., Engel, A., Curtius, J., Birner, T., and Hoor, P.: Quantifying transport into the lowermost stratosphere using simultaneous in-situ measurements of SF_6 and CO_2, Atmos. Chem. Phys., 9, 5905–5919, 2009.

Boucher, O., Friedlingstein, P., Collins, B., and Shine, K. P.: The indirect global warming potential and global temperature change potential due to mothane oxidation, Environ. Res. Lett., 4, https://doi.org/10.1088/1748-9326/4/4/044007, 2009.

Bowman, K. P., Pan, L. L., Campos, T., and Gao, R. S.: Observations of fine-scale transport structure in the upper troposphere from the High-performance Instrument Airborne Platform for Environmental Research, J. Geophys. Res., 112, https://doi.org/10.1029/2007JD008685, 2007.

Collins, W. J., Stevenson, D. S., Johnson, C. E., and Derwent, R. G.: Tropospheric ozone in a global-scale three-dimensional Lagrangian model and its response to NO_x emission controls, J Atmos Chem, 26, 223–274, 1997.

Corti, F., Luo, B. P., Fu, Q., Vömel, H., and Peter, T.: The impact of cirrus clouds on tropical troposphere-to-stratosphere transport, Atmos. Chem. Phys., 6, 1725–1747, 2006.

Dee, D. P., Uppala, S. M., Simmons, A. J., Berrisford, P., Poli, P., Kobayashi, S., Andrae, U., Balmaseda, M. A., Balsamo, G., Bauer, P., Bechtold, P., Beljaars, A. C. M., van de Berg, L., Bidlot, J., Bormann, N., Delsol, C., Dragani, R., Fuentes, M., Geer, A. J., Haimberger, L., Healy, S. B., Hersbach, H., Holm, E. V., Isaksen, L., Kallberg, P., Kohler, M., Matricardi, M., McNally, A. P., Monge-Sanz, B. M., Morcrette, J. J., Park, B. K., Peubey, C., de Rosnay, P., Tavolato, C., Thepaut, J. N., and Vitart, F.: The ERA-Interim reanalysis: configuration and performance of the data assimilation system, Q. J. R. Meteorol. Soc., 137, 553–597, https://doi.org/10.1002/qj.828, 2011.

Diallo, M., Legras, B., Ray, E., Engel, A., and Anel, J.: Global distribution of CO_2 in the upper troposphere and stratosphere, Atmos. Chem. Phys., 17, 3861–3878, https://doi.org/10.5194/acp-17-3861-2017, 2017.

Emanuel, K.: Atmospheric convection, Oxford University Press, New York, 1994.

Emanuel, K. A.: A scheme for representing cumulus convection in large-scale models, J. Atmos. Sci., 48, 2313 – 2335, 1991.

Ertel, H.: Methoden und Probleme der dynamischen Meteorologie, Springer, 1938.

Fairlie, T. D., Pierce, R. B., Al-Saadi, J. A., Grose, W. L., Russell, J. M., Proffitt, M. H., and Webster, C. R.: The contribution of mixing in Lagrangian Photochemical predictions of polar ozone loss over the Arctic in summer 1997, J. Geophys. Res., 104, 26 597–26 609, 1999.

Garny, H., Birner, T., Bönisch, H., and Bunzel, F.: The effects of mixing on Age of Air, J. Geophys. Res., 119, https://doi.org/10.1002/2013JD021417, 2014.

Gettelman, A. and de Forster, P. M.: Definition and climatology of the tropical tropopause layer, jmsj, 80:4B, 911–924, 2002.

Konopka, P. and Pan, L. L.: On the mixing-driven formation of the Extratropical Transition Layer (ExTL), J. Geophys. Res., 117, https://doi.org/10.1029/2012JD017876, 2012.

10   Konopka, P., Steinhorst, H.-M., Grooß, J.-U., Günther, G., Müller, R., Elkins, J. W., Jost, H.-J., Richard, E., Schmidt, U., Toon, G., and
McKenna, D. S.: Mixing and Ozone Loss in the 1999-2000 Arctic Vortex: Simulations with the 3-dimensional Chemical Lagrangian
Model of the Stratosphere (CLaMS), J. Geophys. Res., 109, D02315, https://doi.org/10.1029/2003JD003792, 2004.

Konopka, P., Günther, G., Müller, R., dos Santos, F. H. S., Schiller, C., Ravegnani, F., Ulanovsky, A., Schlager, H., Volk, C. M., Viciani, S.,
Pan, L. L., McKenna, D.-S., and Riese, M.: Contribution of mixing to upward transport across the tropical tropopause layer (TTL), Atmos.
15   Chem. Phys., 7, 3285–3308, 2007.

Konopka, P., Ploeger, F., and Müller, R.: Entropy- and static stability-based Lagrangian model grids, vol. 200, pp. 99–109, American Geo-
physical Union, Washington, DC, Geophys. Monogr., https://doi.org/10.1029/95GL00814, 2012.

Legras, B., Pisso, I., Berthet, G., and Lefevre, F.: Variability of the Lagrangian turbulent diffusion in the lower stratosphere, Atmos. Chem.
Phys., 5, 1605–1622, 2005.

20   Machida, T., Kita, K., Kondo, Y., Blake, D., Kawakami, S., Inoue, G., and Ogawa, T.: Vertical and Meridional Distributions of the
Atmospheric CO_2 Mixing Ratio between Northern Midlatitudes and Southern Subtropics, Journal of Geophysical Research, 108,
https://doi.org/10.1029/2001JD000910, 2002.

Machida, T., Matsueda, H., Sawa, Y., Nakagawa, Y., Hirotani, K., Kondo, N., Goto, K., Nakazawa, T., Ishikawa, K., and Ogawa, T.: World-
wide Measurements of Atmospheric CO_2 and Other Trace Gas Species Using Commercial Airlines, Journal of Atmospheric and Oceanic
25   Technology, 25, 1744–1754, https://doi.org/10.1175/2008JTECHA1082.1, 2008.

Mahowald, N. M., Plumb, R. A., Rasch, P. J., del Corral, J., and Sassi, F.: Stratospheric transport in a three-dimensional isentropic coordinate
model, J. Geophys. Res., 107, 4254, https://doi.org/10.1029/2001JD001313, 2002.

McKenna, D. S., Grooß, J.-U., Günther, G., Konopka, P., Müller, R., Carver, G., and Sasano, Y.: A new Chemical Lagrangian
Model of the Stratosphere (CLaMS): 2. Formulation of chemistry scheme and initialization, J. Geophys. Res., 107, 4256,
30   https://doi.org/10.1029/2000JD000113, 2002a.

McKenna, D. S., Konopka, P., Grooß, J.-U., Günther, G., Müller, R., Spang, R., Offermann, D., and Orsolini, Y.: A new Chem-
ical Lagrangian Model of the Stratosphere (CLaMS): 1. Formulation of advection and mixing, J. Geophys. Res., 107, 4309,
https://doi.org/10.1029/2000JD000114, 2002b.

Pan, L. L., Atlas, E. L., Salawitch, R. J., Honomichl, S. B., Bresch, J. F., Randel, W. J., Apel, E. C., Hornbrook, R. S., Weinheimer, A. J.,
35   Anderson, D. C., Andrews, S. J., Baidar, S., Beaton, S. P., Campos, T. L., Carpenter, L. J., Chen, D., Dix, B., Donets, V., Hall, S. R.,
Hanisco, T. F., Homeyer, C. R., Huey, L. G., Jensen, J. B., Kaser, L., Kinnison, D. E., Koenig, T. K., Lamarque, J.-F., Liu, C., Luo, J., Luo,
Z. J., Montzka, D. D., Nicely, J. M., Pierce, R. B., Riemer, D. D., Robinson, T., and Romashkin, P.: The Convective Transport of Active
Species in the Tropics (CONTRAST) Experiment, Bull. Am. Meteorol. Soc., 98, 106–128, 2017.

Park, M., Randel, W. J., Kinnison, D. E., Emmons, L. K., Bernath, P. F., Walker, K. A., Boone, C. D., and Livesey, N. J.: Hydrocarbons in the
upper troposphere and lower stratosphere observed from ACE-FTS and comparisons with WACCM, J. Geophys. Res., 118, 1964–1980,
2013.

5   Peters, W., Jacobson, A. R., Sweeney, C., Andrews, A. E., Conway, T. J., Masarie, K., Miller, J. B., Bruhwiler, L. M. P., Petron, G., Hirsch,
A. I., Worthy, D. E. J., van der Werf, G. R., Randerson, J. T., Wennberg, P. O., Krol, M. C., and Tans, P. P.: An atmospheric perspective on
North American carbon dioxide exchange: CarbonTracker, Proc. Natl. Acad. Sci., 104, 18 925 – 18 930, 2007.

Ploeger, F., Konopka, P., Günther, G., Grooß, J.-U., and Müller, R.: Impact of the vertical velocity scheme on modeling transport across the
tropical tropopause layer, J. Geophys. Res., 115, D03301, https://doi.org/10.1029/2009JD012023, 2010.

10 Pommrich, R., Müller, R., Grooß, J.-U., Konopka, P., Ploeger, F., Vogel, B., Tao, M., Hoppe, C., Günther, G., Spelten, N., et al.: Tropical tro-
posphere to stratosphere transport of carbon monoxide and long-lived trace species in the Chemical Lagrangian Model of the Stratosphere
(CLaMS), Geoscientific Model Development, 7, 2895–2916, 2014.

Poshyvailo, L., Müller, R., Konopka, P., Günther, G., Riese, M., Podglajen, A., and Ploeger, F.: Sensitivities of modelled water vapour in the
lower stratosphere: temperature uncertainty, effects of horizontal transport and small-scale mixing, Atmos. Chem. Phys., 18, 8505–8527,
15   2018.

Prather, M., Zhu, X., Tang, Q., Hsu, J., and Neu, J.: An atmospheric chemist in search of the tropopause, J. Geophys. Res., 116, 2011.

Pugh, T. A. M., Cain, M., Methven, J., Wild, O., Arnold, S. R., Real, E., Law, K. S., Emmerson, K. M., Owen, S. M., Pyle, J. A., Hewitt,
C. N., and MacKenzie, A. R.: A Lagrangian model of air-mass photochemistry and mixing using a trajectory ensemble: the Cambridge
Tropospheric Trajectory model of Chemistry And Transport (CiTTyCAT) version 4.2, Geosci. Model Dev., 5, 193–221, 2012.

20 Reithmeier, C. and Sausen, R.: ATTILA - Atmospheric Tracer Transport in a Lagrangian Model, Tellus B, 54, 278–299,
https://doi.org/10.1034/j.1600-0889.2002.01236.x, 2002.

Riese, M., Ploeger, F., Rap, A., Vogel, B., Konopka, P., Dameris, M., and Forster, P. M.: Impact of uncertainties in atmospheric mixing on
simulated UTLS composition and related radiative effects, J. Geophys. Res., 117, D16, https://doi.org/doi:10.1029/2012JD017751, 2012.

Russo, M. R., Marecal, V., C. R. Hoyle and, J. A., Chemel, C., Chipperfield, M. P., Dessens, O., Feng, W., Hosking, J. S., Telford, P. J., Wild,
25   O., Yang, X., , and Pyle, J. A.: Representation of tropical deep convection in atmospheric models (Part 1): Meteorology and comparison
with satellite observations, Atmos. Chem. Phys., 11, 2765–2786, 2011.

Salby, M. L.: Fundamentals of atmospheric physics, Academic Press, San Diego, 1996.

Sawa, Y., Machida, T., Matsueda, H., Niwa, Y., Tsuboi, K., Murayama, S., Morimoto, S., and Aoki, S.: Seasonal changes of CO_2, CH_4, N_2O
and SF_6 in the upper troposphere/lower stratosphere over the Eurasian continent observed by commercial airliner, Geophys. Res. Lett.,
30   42, 2001–2008, https://doi.org/10.1002/2014GL062734, 2015.

Schiller, C., Afchine, A., Eicke, N., Feigl, C., Fischer, H., Giez, A., Konopka, P., Schlager, H., Tuitjer, F., and Zöger, F. G. W. M.: Ice particle
formation and sedimentation in the tropopause region: A case study based on in situ measurements of total water during POLSTAR1997,
Geophys. Res. Lett., 26, 2219 – 2222, https://doi.org/10.1029/1999GL900337, 1999.

Stohl, A., Forster, C., Frank, A., Seibert, P., and Wotawa, G.: Technical note: The Lagrangian particle dispersion model FLEXPART version
35   6.2, Atmos. Chem. Phys., 5, 2461–2474, 2005.

Stull, R. B.: An introduction to boundary layer meteorology, vol. 13, Springer Science & Business Media, 1988.

Tao, M., Pan, L. L., Konopka, P., Honomichl, S. B., Kinnison, D. E., and Apel, E. C.: A Lagrangian model diagnosis of stratospheric
contributions to tropical mid-tropospheric air, J. Geophys. Res., almost accepted, 2018.

Tiedtke, M.: A comprehensive mass flux scheme for cumulus parameterization in large-scale models, Mon. Wea. Rev., 117, 1779–1800,
1989.

Turner, J. S.: Buoyancy Effects in Fluids, Cambridge University Press, 1973.

Vallis, G. K.: Atmospheric and oceanic fluid dynamics: fundamentals and large-scale circulation, Cambridge University Press, 2006.

560 Vogel, B., Pan, L. L., Konopka, P., Günther, G., Müller, R., Campos, T., Hall, W., Pollack, I., Weinheimer, A., Wei, J., Atlas, E. L., and
Bowman, K. P.: Transport pathways and signatures of mixing in the extratropical tropopause region derived from Lagrangian model
simulations, J. Geophys. Res., 116, https://doi.org/10.1029/2010JD014876, 2011.

Waugh, D. W. and Hall, T. M.: Age of stratospheric air: Theory, observations, and models, Rev. Geophys., 40, 1–27, 2002.

Wernli, H. and Davies, H. C.: A Lagrangian-based analysis of extratropical cyclones I: The method and some applications, Q. J. R. Meteorol.
565   Soc., 123, 467–489, 1997.

Wohltmann, I. and Rex, M.: The Lagrangian chemistry and transport model ATLAS: validation of transport and mixing, Geosci. Model Dev.,
        2, 153–173, 2009.